Environmental Science
ISSN : 2028-2508
e-ISSN : 2737-890X
CODEN : JMESCN

J. Mater. Environ. Sci., **2025, Volume 16, Issue 9, Page 1622-1640**

http://www.jmaterenvironsci.com

Monitoring Anopheles Mosquitoes Through Lidar, Weather, and Vegetation Index Data Analysis: A Study in Côte d'Ivoire

Assoumou S. Doria Yamoa [1*], Benoit K. Kouakou[1,2], Adolphe Y. Gbogbo[1], Jeremie T. Zoueu[1,2]

[1] *Instrumentation, Imaging and Spectroscopy Laboratory, Félix Houphouët-Boigny Polytechnic Institute, Yamoussoukro, Ivory Coast*

[2] *Dept. Physics, University of San Pedro, San Pedro, Ivory Coast*

**Corresponding author: Assoumou S. Doria Yamoa, Email address: assoumou.yamoa21@inphb.ci*

Received *25 June 2025,*
Revised *03 Aug 2025,*
Accepted *05 Aug 2025*

Citation*: Yamoa A.S.D., Kouakou B.K., Gbogbo A.Y., Zoueu J. T. (2025) Monitoring Anopheles Mosquitoes Through Lidar, Weather, and Vegetation Index Data Analysis: A Study in Côte d'Ivoire, J. Mater. Environ. Sci., 16(9), 1622-1640*

Abstract: Malaria remains a major public health burden in Côte d'Ivoire. Effective surveillance of Anopheles vectors is essential but limited by traditional methods. This study evaluates an integrated approach combining an entomological Lidar based on the Scheimpflug principle, local meteorological data, and vegetation indices derived from Sentinel-2 to monitor Anopheles across five ecologically distinct sites in Côte d'Ivoire (urban, agricultural, peri-urban, forest). A descriptive and exploratory analysis of Light Detection and Ranging (Lidar) data (wingbeat frequency - WBF), meteorological data (temperature, humidity, wind), and vegetation indices (Normalized Difference Vegetation Index (NDVI), Normalized Difference Water Index (NDWI), Chlorophyll Index (IC), Modified Soil Adjusted Vegetation Index (MSAVI), Normalized Difference Moisture Index (NDMI), Normalized Difference Red Edge (NDRE)) was conducted using Python. The results show significant spatiotemporal heterogeneity in the abundance of Lidar signals attributed to Anopheles. Abundance peaks during the short rainy season, particularly at the Center, Farm, and North sites. Activity throughout the 24-hour cycle shows marked evening peaks (6–8 p.m. (18:00 to 20:00)) at most sites, correlated with temperature and humidity. The distribution of WBF appears relatively stable despite large fluctuations in abundance. Average vegetation indices per site suggest a link between vegetation cover/humidity and observed abundance. This integrated approach offers a promising method for detailed and context-specific surveillance of malaria vectors, enabling the identification of spatiotemporal "hotspots" and informing vector control strategies.

Keywords: *Anopheles*, Vector Surveillance, Scheimpflug Lidar, Meteorology, Vegetation Indices, Spatiotemporal

1. Introduction

Malaria remains a major public health issue in sub-Saharan Africa, and Côte d'Ivoire is no exception (Manta 2025; Roméo et al. 2022; Soma et al. 2020). Mosquitoes of the genus Anopheles are the primary vectors of this disease (Adja et al. 2022; Djamouko-Djonkam et al. 2019; Fournet et al. 2022; Manta 2025; Taconet et al. 2024; USAID 2024), and effective monitoring of their populations is crucial for implementing targeted vector control strategies. Traditional surveillance methods face limitations in terms of spatial and temporal coverage, cost, and potential biases (Brydegaard et al. 2020;

Chaki et al. 2012; Jansson et al. 2021; Le Breton et al. 2025). In response to these challenges, innovative approaches integrating remote sensing technologies such as Lidar (Gbogbo et al. 2022; Jansson et al. 2021; Kouakou et al. 2020), meteorological data analysis (Tahir et al. 2023), and vegetation indices (Achee et al. 2006; Liu and Chen 2006; Stein et al. 2023; Youssefi et al. 2022), offer significant potential for improving Anopheles surveillance (Frake et al. 2020).

The general objective of this study is to evaluate the effectiveness of Anopheles surveillance through the combined analysis of Lidar, meteorological, and vegetation index data in selected areas of Côte d'Ivoire. The specific objectives include: identifying the presence and activity patterns of Anopheles mosquitoes using Lidar data; correlating this data with local weather conditions; and analyzing the relationship between vegetation indices and Anopheles presence. The central issue of this study is to determine whether an integrated approach—combining Lidar, meteorological, and vegetation index data—can provide a more effective and informative method of Anopheles surveillance than traditional methods typically used.

The hypothesis to be tested is that there is a significant correlation between Anopheles mosquito activity detected by Lidar and specific meteorological conditions (e.g., increased activity during warm and humid periods following rainfall) as well as vegetation indices (e.g., higher abundance in densely vegetated areas favorable to resting and breeding) across the different ecological zones within Côte d'Ivoire. The research question is: How are variations in meteorological conditions and vegetation indices, measured through remote sensing methods, associated with the abundance and activity of Anopheles mosquitoes detected by Lidar in the various studied ecological environments?

This study aims to provide a clear answer to this question by analyzing integrated datasets and assessing the reliability of this method for monitoring Anopheles proliferation. The results will enhance our understanding of the factors influencing Anopheles proliferation and contribute to the development of more effective monitoring and control strategies.

2. Materials and Methods

2.1. Data Collection Sites

This study was conducted across five distinct sites, selected to represent a diversity of environmental conditions potentially influencing *Anopheles* proliferation (**Figure 1**). The study sites are as follows:

- **a) INP NORTH** (6.891070° N, -5.221719° E; measurements from 17/09/2020 to 21/09/2020),
- **b) INP FARM** (6.887991° N, -5.221063° E; measurements from 24/10/2020 to 30/10/2020),
- **c) INP CENTER** (6.868363° N, -5.234445° E; measurements from 07/11/2020 to 15/11/2020),
- **d) INP SOUTH** (6.873785° N, -5.235951° E; measurements from 15/12/2020 to 20/12/2020),
- **e) TAI FOREST or TAI** (5.83345° N, -7.34221° E; measurements from 11/01/2023 to 15/01/2023).

Data collection was based on three main methodologies. First, a Lidar system operating under the Scheimpflug principle was used to detect and record characteristics of flying insects, particularly their wingbeat frequency, at each site. Second, an Acurite weather station was deployed at each site during the insect monitoring periods, enabling continuous recording of meteorological parameters such as temperature, humidity, and wind speed. Lastly, the following vegetation indices were calculated from multispectral Sentinel-2 satellite imagery using the Google Earth Engine platform: the Normalized Difference Vegetation Index (NDVI), the Normalized Difference Water Index (NDWI), the Chlorophyll Index (CI), the Modified Soil-Adjusted Vegetation Index (MSAVI), the Normalized Difference Moisture Index (NDMI), and the Normalized Difference Red Edge Index (NDRE). These indices were used to characterize the land cover type at each site in a separate study (not yet submitted).

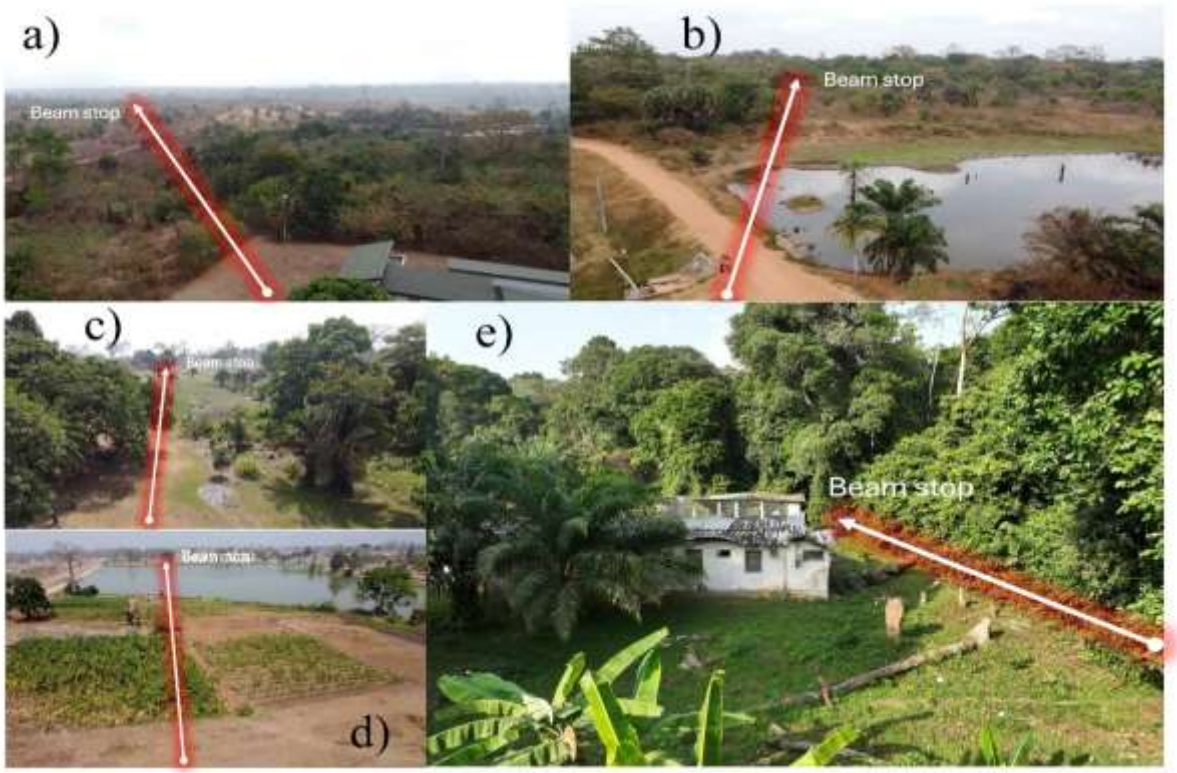

Figure 1. Aerial view of the measurement sites. (a) INP NORTH. (b) INP FARM. (c) INP CENTER. (d) INP SOUTH. (e) TAI FOREST or TAI.

2.2. Experimental Setup

A polarized entomological Lidar system (**Figure 2**), operating based on the Scheimpflug principle, was deployed at each site to study the proliferation of female *Anopheles* mosquitoes. This system, whose technical specifications are detailed in **Table 1**, enables high-resolution imaging over long distances thanks to the precise alignment of its emitter and receiver telescopes.

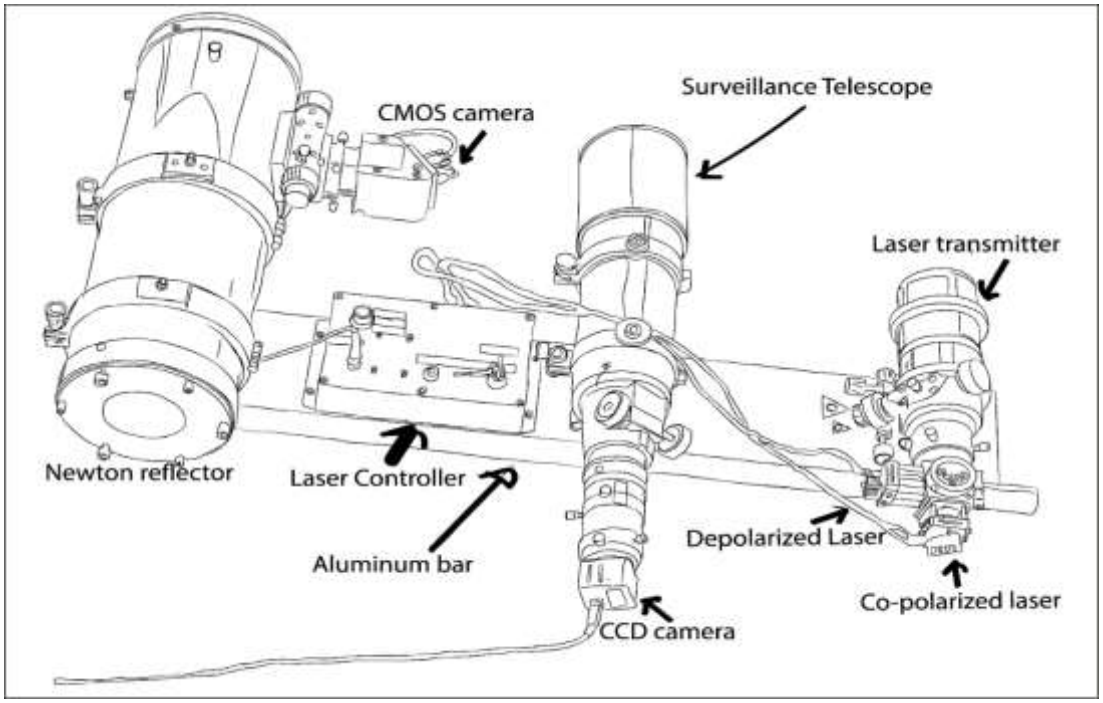

Figure 2. Scheimpflug lidar system drawing.

In brief, the system includes an emitter telescope equipped with a polarization system, a Newtonian reflector receiver telescope, and a data processing unit capable of detecting and characterizing flying insects. Data processing involved several steps: demultiplexing, background subtraction, image cropping, and calibration, resulting in the estimation of the insects' optical cross-section (σ) (Li 2024). This advanced technology offers strong potential for the accurate detection and characterization of flying insects, particularly *Anopheles* mosquitoes.

Table 1. Characteristics of the Scheimpflug Lidar

Characteristic Name	Value	Unit	Function
Optical Principle	Scheimpflug Principle	-	Simultaneous focus on the image plane
Base Distance	814	mm	Determines the geometry between emitter and receiver
Emitter Telescope Diameter	75	mm	Determines the amount of light emitted
Emitter Telescope Focal Length	300	mm	Controls the divergence of the beam
Polarization Type	Co-polarized & depolarized (TE)	-	Analyzes polarization properties of backscatter
Beam Combiner Type	Cube combiner + dichroic mirror	-	Combines the two laser beams
Laser Diode Power	2 × 5	W	Total power of the laser beam
Laser Wavelength	808	nm	Optimized for biological detection
Receiver Telescope Type	Newtonian Reflector	-	Collects backscattered light
Receiver Telescope Diameter	150	mm	Determines the light collected
Receiver Telescope Focal Length	600	mm	Allows precise focusing
CMOS Linear Sensor	2048	Pixels	Spatial resolution
CMOS Tilt	37	°	Scheimpflug condition met
Termination Type	Absorptive target	-	Avoids background interference
Termination Material	Black neoprene	-	Calibrates optical response
Repetition Frequency	10	kHz	Temporal resolution
Scan Frequency	100	µs	Interval between pulses
Pulse Duration	80	µs	Depth resolution
Weight of a 3s File	120	MB	Storage capacity
Intensity Resolution	12	Bits	Precision in intensity measurement
Recording Software	LabVIEW	-	Automated recording
Data Volume/Day	1.1	TB	Daily raw data
Data Reduction	~99%	%	Optimizes storage
Processing Software	MATLAB	-	Post-processing and analysis
Data Format	3 × 2D Matrices	-	Structures data by polarization
Calibration Parameter	Optical Section σ	mm^2	Quantifies the effective surface of insects

2.3. Methodology

In this work, we conducted a thorough descriptive and exploratory analysis of entomological data from different locations and seasons, using Python (v.3.9 and visualization libraries such as Seaborn, Matplotlib, Plotly, and Pandas. After importing and preparing the data (including renaming categorical variables to make them readable), we generated several types of graphs to explore the distribution of insect species according to site, season, temperature, humidity, wind speed, and time. Bar charts,

heatmaps, density plots, boxplots, violin plots, and time series allowed us to visualize the distribution, co-occurrence, and correlations between variables. Particular emphasis was placed on the female Anopheles species (a disease vector), in order to track its spatio-temporal proliferation and its relationship with climatic factors and vegetation indices (NDVI, NDWI, MSAVI, NDRE, CI, NDMI). Descriptive statistics (mean, standard deviation, median, IQR, mode) were also calculated to summarize trends by site and season with regard to the use of Scheimpflug Lidar for vector surveillance. This methodology aims to detect spatial and temporal signatures associated with the proliferation of potential disease vectors, using a data-driven approach.

3. Results

The distribution of different species in relation to temperature–relative humidity pairs can be observed (**Figure 3**). At Site 1 (Center), a wide dispersion of data points is noted, suggesting the presence of all species across a broad range of temperature and relative humidity conditions. However, species 1 and 2 (bees) appear to dominate under lower temperature and humidity conditions. In contrast, species 3 and 4 (*Anopheles* mosquitoes) are present across a wider range, with a noticeable concentration at higher relative humidity values. Similarly, at Site 2 (Farm), the distribution resembles that of Site 1, with a notable presence of species 1 and 2 at lower temperature and humidity values.

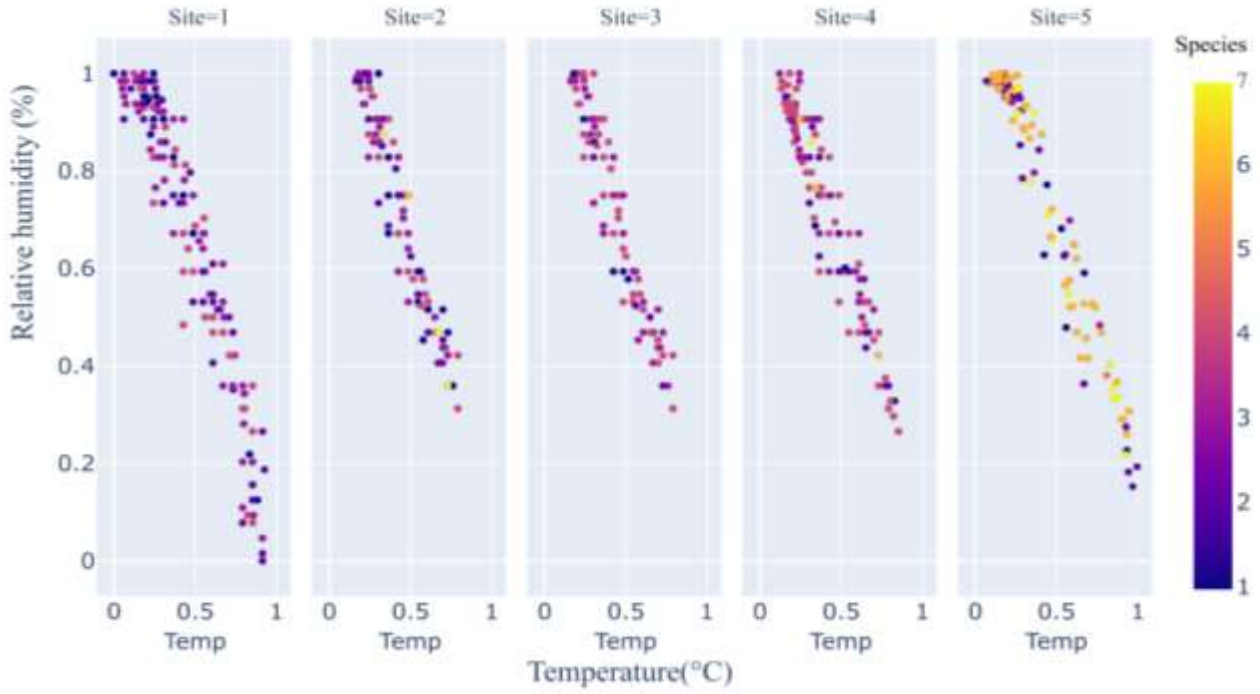

Figure 3. Relationship Between Temperature, Relative Humidity, and Species by Site. This figure presents five side-by-side scatter plots, each corresponding to one of the study sites (Site 1: Center, Site 2: Farm, Site 3: North, Site 4: South, Site 5: Tai). In each plot, the x-axis represents temperature (Temp) and the y-axis represents relative humidity (Rhum), both normalized on a scale from 0 to 1. Each point represents an individual observation, and its color indicates the species identified, following a gradient from violet to yellow. The color scale includes: violet for Species 1 (*Apis mellifera*, Domestic Bee), blue for Species 2 (Wild Bee), green for Species 3 (Female *Anopheles*), orange for Species 4 (Male *Anopheles*), red for Species 5 (Grasshopper), light red for Species 6 (Dragonfly), and yellow for Species 7 (Butterfly).

Anopheles (species 3 and 4) are also present across a broad spectrum, with a slight tendency to cluster under higher humidity conditions. In contrast, Site 3 (North) shows a somewhat different distribution. Species 1 and 2 are markedly present in the lower-left section of the graph (low temperature and relative humidity). Species 3 and 4 are also present, but perhaps within a slightly different range of environmental conditions compared to Sites 1 and 2. Moreover, species 5, 6, and 7 appear to be more limited or concentrated in specific areas of the diagram. At Site 4 (South), there is a greater concentration of points at higher relative humidity values across several species. While species 1 and 2 are still observed in low temperature and humidity conditions, the proportion of other species—especially *Anopheles*—appears to increase under humid conditions. Finally, Site 5 (Tai) shows a distribution spanning a wide range of temperatures, with a predominance of species 6 and 7 (dragonflies and butterflies) in the upper part of the graph, suggesting a potential association with higher relative humidity. Although *Anopheles* (species 3 and 4) are also present, their relative distribution compared to other species differs from that observed at the other sites.

Figure 4-a shows notable variations in the number of observations by species and site. At Site 1 (Center), Species 3 (Female *Anopheles*) had the highest number of observations, followed by Species 4 (Male *Anopheles*), while other species were recorded in much lower numbers. A similar pattern was observed at Site 2 (Farm), though with slightly fewer total observations for *Anopheles* species compared to Site 1. Site 3 (North) exhibited the highest abundance of Species 3 and 4 among all sites, while non-*Anopheles* species remained relatively scarce. At Site 4 (South), although *Anopheles* mosquitoes were still the most abundant, the gap between them and other species was less pronounced, with a comparatively higher presence of Species 6 (Dragonfly). In contrast, Site 5 (Tai) stood out with significantly fewer *Anopheles* observations, while Species 6 had a relatively higher presence than at Sites 1, 2, and 3. **Figure 4-b** illustrates species distribution across seasons. During Season 1 (Short dry season), *Anopheles* species were still present in significant numbers, but Species 2 (Wild Bee) reached its highest relative abundance. Season 2 (Short rainy season) was marked by a surge in observations of Species 3 and 4, far exceeding counts in other seasons, with other species also increasing but to a lesser extent. In Season 3 (Long dry season), *Anopheles* counts dropped sharply, reaching levels similar to or lower than those in Season 1, while Species 6 (Dragonfly) reached its peak relative abundance during this period.

Figure 5-a shows the seasonal distribution of species observations. During Season 1 (Short dry season), Species 2 (Wild Bee) and Species 3 (Female Anopheles) recorded relatively higher observation counts compared to the other species. Season 2 (Short rainy season) is marked by a dramatic surge in observations of Species 3 and 4 (Anopheles Female and Male), far surpassing other species and seasons, with Species 2 also showing a notable presence. In contrast, Season 3 (Long dry season) is characterized by generally lower observation counts across most species; however, Species 5 (Grasshopper), 6 (Dragonfly), and 7 (Butterfly) were relatively more present than Anopheles during this period.

Figure 5-b focuses specifically on Female Anopheles proliferation by site and season. In Season 1, Site 3 (North) recorded a relatively high number of Female Anopheles observations compared to the other sites. In Season 2, Sites 1 (Center) and 2 (Farm) showed the highest levels of Anopheles proliferation, with maximum observation counts, while Site 3 also maintained high counts. During Season 3, Female Anopheles observations dropped sharply, with most sites recording very low or no activity. The only data for this season came from Site 4 (South), which recorded a low count (1,165), and Site 5 (Tai), where the number of observations was minimal (144).

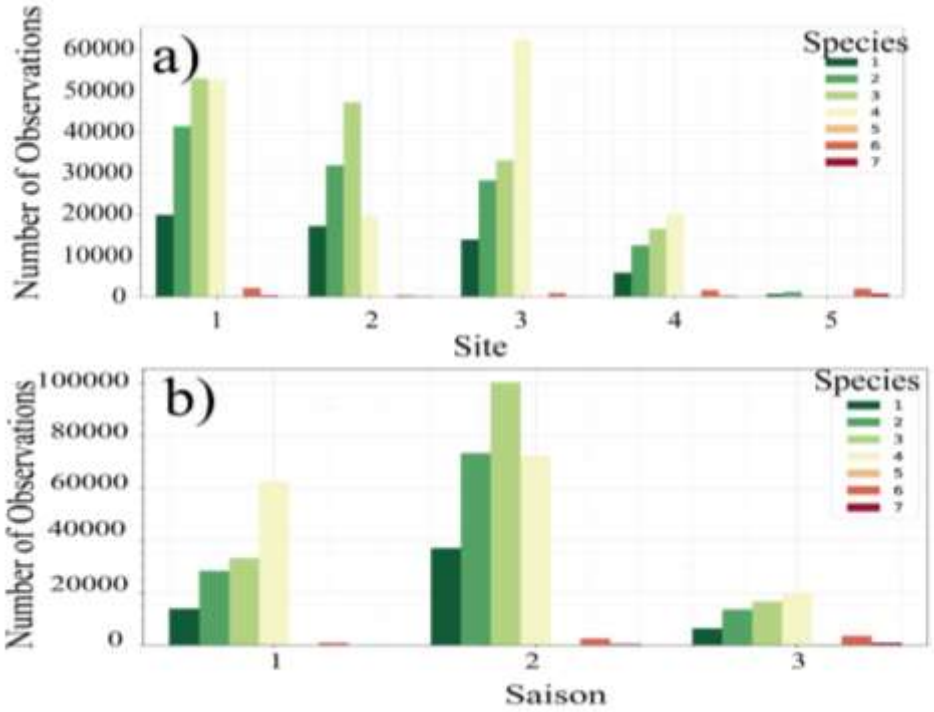

Figure 4. Observation Abundance by Species According to Site and Seasons. In panel (a), the x-axis represents the five study sites (1 to 5), while the y-axis shows the number of observations, ranging from 0 to 60,000. At each site, a group of seven adjacent bars represents the seven recorded species—1: Domestic Bee, 2: Wild Bee, 3: Female *Anopheles*, 4: Male *Anopheles*, 5: Grasshopper, 6: Dragonfly, and 7: Butterfly—each assigned a specific color according to the legend. In panel (b), the x-axis corresponds to the three seasons (1: Short dry season, 2: Short rainy season, 3: Long dry season), and the y-axis displays the number of observations from 0 to 100,000. Similar to panel (a), each season features a group of seven colored bars representing the same species using the same color coding.

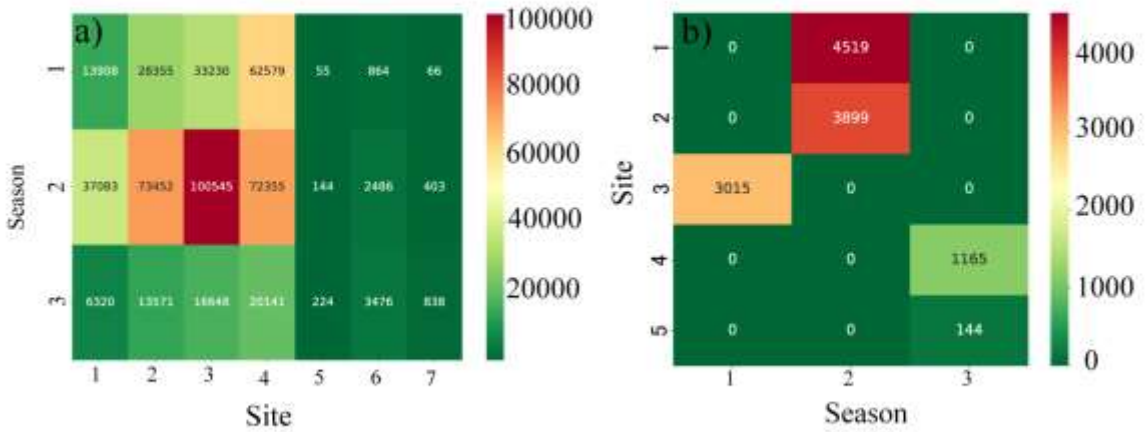

Figure 5. Species Distribution by Season (Heatmap) and Female Anopheles Proliferation by Site and Season. In panel (a), the vertical axis represents the three seasons—1: Short dry season, 2: Short rainy season, and 3: Long dry season—while the horizontal axis shows the seven species (1 to 7). Each cell in the heatmap is color-coded based on the number of observations for a given species during a specific season, using a color gradient from green (low observation count) to red (high observation count), as indicated by the color scale on the right. The exact number of observations is also displayed within each cell. Panel (b) focuses on the seasonal proliferation of Female *Anopheles* (Species 3) across the five sites. The vertical axis represents the five sites (1 to 5), and the horizontal axis represents the three seasons (1 to 3). Each cell is colored according to the number of observations of Female *Anopheles* recorded at a specific site during a given season, using the same green-to-red color scale. Numeric observation values are also shown in each cell for clarity.

Figure 6-a presents violin plots illustrating the distribution of *Anopheles* wingbeat frequency across the five study sites. Sites 1, 2, 3, and 4 display similar overall shapes, suggesting comparable frequency distributions, while Site 5 shows a slightly broader spread. The medians (white lines) for Sites 1, 3, and 4 cluster around 0.52, slightly lower at Site 2 (≈0.50), and lowest at Site 5 (≈0.49). Interquartile ranges (IQRs) are similar for Sites 1, 3, and 4, while Sites 2 and 5 show slightly narrower IQRs, indicating reduced variability in the central 50% of values. Whiskers extend similarly across all sites, with minimum values near 0.417 and maximums near 0.643, slightly lower for Site 5. Descriptive statistics (**Table 2**) confirm these patterns: mean frequencies hover around 0.52 for Sites 1, 3, and 4, slightly lower for Site 2 (0.511), and lowest at Site 5 (0.508). Standard deviations are low and consistent (≈0.065), reflecting stable dispersion, while Site 5 has significantly fewer observations. The mode remains constant at 0.474 for Sites 1, 3, and 4, lower for Site 2 (0.425), and lowest at Site 5 (0.417).

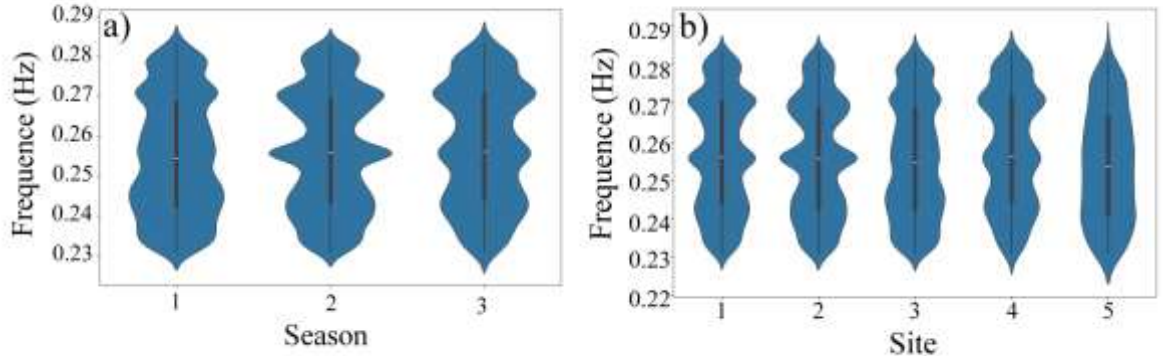

Figure 6. Distribution and Statistics of Anopheles Wingbeat Frequency by Site and Season. Panel (a) displays the frequency distribution by site. The horizontal axis shows the five study sites (1 to 5), and the vertical axis represents wingbeat frequency, ranging from 0.22 to 0.29. Each violin plot visualizes the density of frequency values for a given site, with wider sections indicating higher data concentration. A white horizontal line marks the median, while a black box at the center represents the interquartile range (IQR). Thin lines (whiskers) extend from the box to show the full spread of the data, typically up to 1.5 times the IQR. Accompanying descriptive statistics for each site include the number of observations, mean, median, standard deviation, minimum, maximum, first quartile (Q1), third quartile (Q3), mode, and IQR. Panel (b) mirrors the same structure for seasonal analysis. The horizontal axis indicates the three seasons (1: short dry season, 2: short rainy season, 3: long dry season), with violin plots illustrating the frequency distribution of *Anopheles* per season. Similar statistical summaries are provided, allowing for direct comparison of frequency dynamics across both spatial and seasonal dimensions.

Table 2. Statistic by Site

Site	Count	Mean	Median	Std. Dev.	Min	Max	Q1	Q3	Mode	IQR
1	53184	0.5243	0.5221	0.0651	0.4173	0.6432	0.4681	0.5812	0.4740	0.1131
2	47361	0.5112	0.5016	0.0640	0.4173	0.6431	0.4547	0.5625	0.4252	0.1078
3	33230	0.5251	0.5209	0.0655	0.4173	0.6432	0.4694	0.5839	0.4740	0.1145
4	16483	0.5208	0.5152	0.0652	0.4173	0.6432	0.4645	0.5781	0.4740	0.1136
5	165	0.5076	0.4885	0.0676	0.4174	0.6404	0.4491	0.5623	0.4174	0.1132

Figure 6-b shows violin plots by season. All three seasons exhibit similar shapes, though Season 2 (short rainy season) appears slightly wider at the center, suggesting denser data concentration around the median. Medians are close across all seasons (≈0.512 to 0.521), with nearly identical IQRs and

whisker ranges. Descriptive statistics (**Table 3**) reinforce the visual analysis: mean frequencies range from 0.518 to 0.525, standard deviations remain low and uniform (~0.065), and Season 2 contains the highest number of observations. The mode is 0.474 for Seasons 1 and 3, and slightly lower at 0.425 for Season 2. Overall, the frequency distributions of *Anopheles* are relatively stable across sites and seasons, despite variations in abundance.Similar observations were made in **Figure 7.** First, at Site 1 (Center), female *Anopheles* abundance shows main peaks in the early evening (around 6:00 PM to 8:00 PM) and a secondary peak in the early morning (around 6:00 AM).

Table 3. Statistics by Season

Season	Count	Mean	Median	Std. Dev	Min	Max	Q1	Q3	Mode	IQR
1	33230	0.5251	0.5209	0.0655	0.4173	0.6432	0.4695	0.5839	0.4740	0.1145
2	100545	0.5182	0.5123	0.0649	0.4173	0.6432	0.4610	0.5738	0.4252	0.1128
3	16648	0.5207	0.5151	0.0652	0.4173	0.6432	0.4643	0.5780	0.4740	0.1137

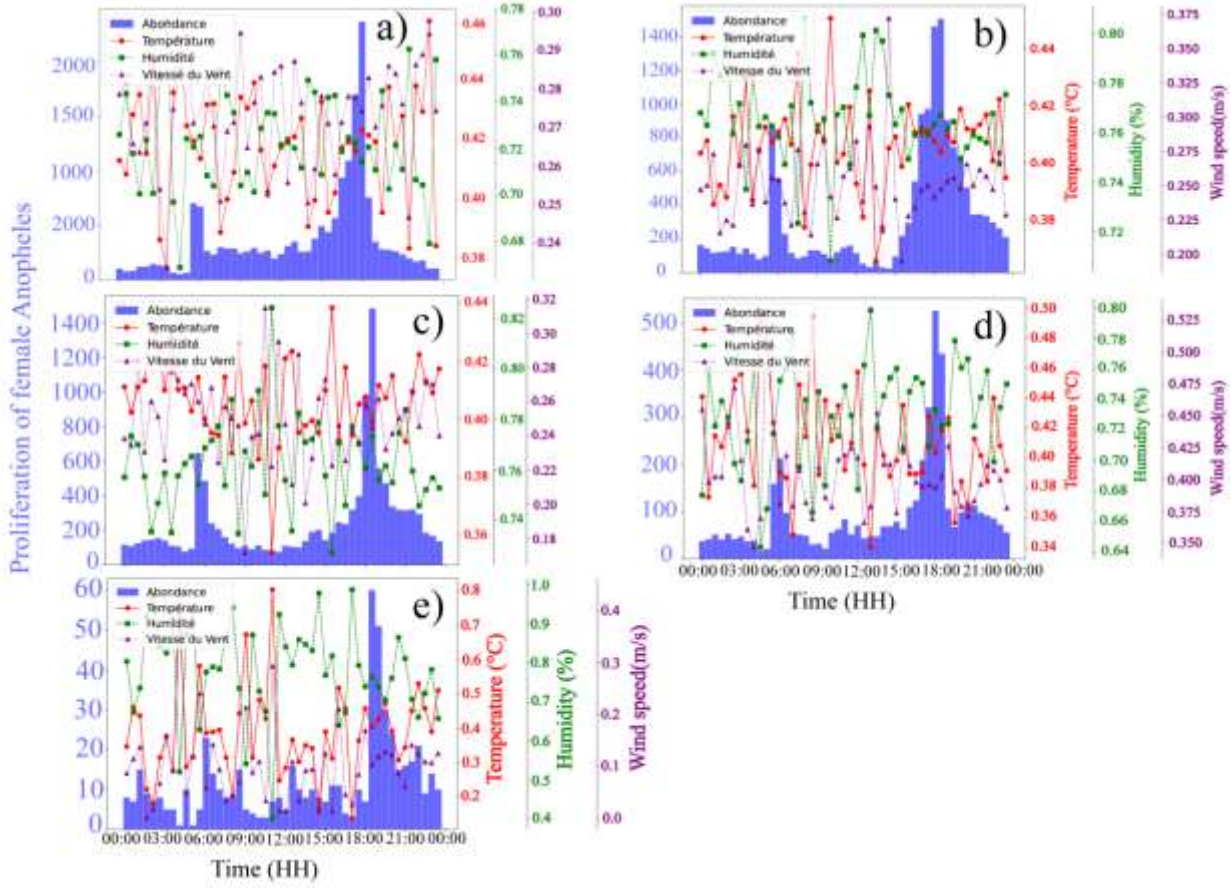

Figure 7. Female Anopheles Abundance and meteorological parameters in 3 hours Intervals by Site. This figure is composed of five individual subplots (a, b, c, d, e), each representing one of the five study sites. Each plot displays the variation over a 24-hour period of female *Anopheles* abundance (blue bars) alongside three meteorological parameters: temperature (red solid line with dots), relative humidity (green dotted line with squares), and wind speed (purple dashed line with triangles). The x-axis represents time of day, from 00:00 to 00:00, in 3-hour intervals. The primary y-axis on the left indicates the number of female *Anopheles* (Abundance), while a secondary y-axis on the right shows the values of the meteorological parameters. Temperature and humidity are normalized, ranging from 0.0 to 1.0, and wind speed is plotted on a specific scale that is not explicitly stated but visually ranges from 0 to approximately 0.4.

At the same time, temperature remains relatively stable, with a slight increase around midday. In contrast, humidity is higher at night and decreases during the day. Additionally, wind speed is generally low with occasional spikes. It is noteworthy that the abundance peaks appear to coincide with periods of still relatively high temperatures and decreasing or stable humidity after sunset. Second, at Site 2 (Farm), a similar pattern is observed, with an evening abundance peak (around 6:00 PM to 8:00 PM) and notable activity in the early morning. Likewise, temperature and humidity follow inverse diurnal trends. Wind speed also remains generally low. As with Site 1, the evening activity peak seems to occur when temperature remains high and humidity begins to rise or stabilizes. Third, at Site 3 (North), a very pronounced peak in abundance is observed in the evening (around 6:00 PM to 8:00 PM), with lower activity throughout the rest of the night and morning. Again, the temperature and humidity trends are similar to those at other sites. Importantly, the abundance peak coincides with the time when temperature is still elevated and humidity begins to rise after the heat of the day. Fourth, at Site 4 (South), abundance is more spread out across the night, with a notable peak in the early evening and persistent activity through to the middle of the night. As before, temperature and humidity follow typical diurnal patterns. It is possible that *Anopheles* activity appears less concentrated around a single peak and could be influenced by a combination of meteorological factors over a longer period. Fifth, at Site 5 (Tai), female *Anopheles* abundance is overall much lower at this site. Nevertheless, some activity is observed in the early evening and during the night.

Figure 8 investigates the short-term temporal relationship between female *Anopheles* abundance and vegetation indices, which serve as indicators of land cover and vegetation health, as outlined in **Table 3.** Although no immediate 30-minute-scale correlation is apparent, analysis of average index values by site—referencing **Table 4**—yields meaningful insights regarding habitat influence. At the Center site, high average values of IC and MSAVI suggest healthy, dense vegetation, while the NDVI indicates a moderate to potentially forested landscape. Despite NDWI pointing to generally dry conditions, the overall mix may provide shaded, ground-level microhabitats favorable to *Anopheles*. Similarly, at the Farm site, elevated IC and MSAVI also indicate dense vegetation, with NDVI again suggesting moderate to forested cover. The NDMI points to mid-level forest canopy with varying water stress (Amin I.S. & Amin H.S., 2024; Laita et al., 2024). At the same time, NDWI shows dry to moderately dry conditions—yet agricultural activity may create temporary breeding sites and provide adult resting zones. At the North site, IC, MSAVI, and NDVI also reflect dense, healthy vegetation, with NDMI indicating similar hydric stress, and NDWI pointing to dryness. Even so, dense vegetation may foster humid microclimates conducive to mosquito survival. In contrast, the South site exhibits lower IC and MSAVI values, signaling less vigorous vegetation (germination stage per MSAVI) and a more moderate NDVI. While NDMI indicates medium canopy with variable moisture stress, NDWI shows moderately dry conditions, suggesting reduced adult resting sites but potential for temporary larval habitats. Finally, at the Tai site, IC, MSAVI, and NDVI reflect dense, healthy forested vegetation, and NDMI shows a medium canopy under stress, yet NDWI again suggests dryness—potentially limiting *Anopheles* proliferation despite favorable vegetation structure.

Figure 9 is composed of two parts. Panel (a) illustrates the density of co-occurrence between species and sites. It reveals a high co-occurrence density for species 3 (Female Anopheles) and 4 (Male Anopheles) with sites 1 (Center), 2 (Farm), and 3 (North), indicating a notable abundance of these species in these locations. Site 5 (Tai) shows a low co-occurrence density with all species, suggesting a generally lower abundance—consistent with previous observations (**Figures 4 and 5**)—with only a slight co-occurrence for species 6 (Dragonfly).

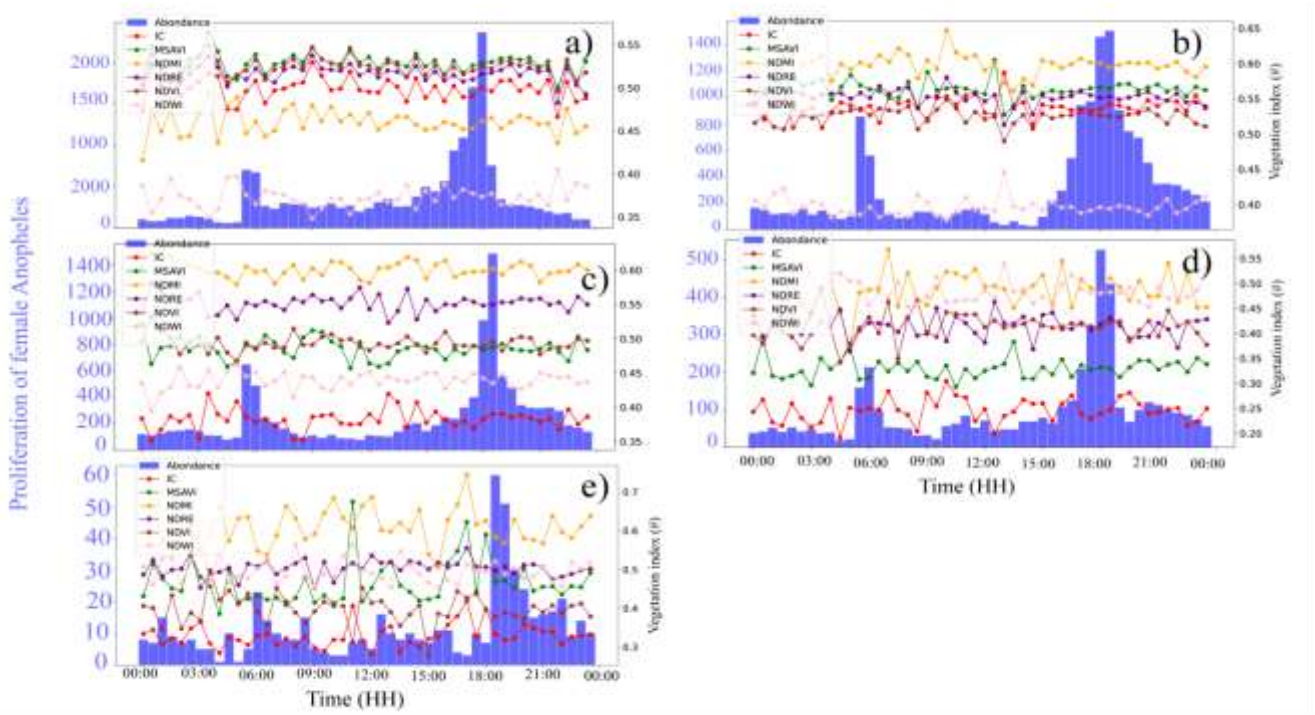

Figure 8. Female Anopheles Abundance and vegetation indices at 3 hours intervals for each site. She presents five individual plots (a to e), each corresponding to one of the five study sites. Each plot illustrates the evolution of female *Anopheles* abundance (blue bars) alongside six vegetation indices over a 24-hour period, with data recorded at 30-minute intervals. These indices include IC (red line with dots), MSAVI (green line with dots), NDMI (yellow line with dots), NDRE (brown line with dots), NDVI (purple line with dots), and NDWI (light pink line with dots). The horizontal axis represents the time of day (from 00:00 to 00:00), while the left vertical axis indicates the number of female *Anopheles* (Abundance). A secondary vertical axis on the right displays the vegetation index values, which range approximately from 0.2 to 0.7.

Table 4. Interpretation of Ground Cover Based on Vegetation Index

Site	Index	Average	Maximum	Interpretation (Average)	Interpretation (Maximum)
Center	IC	1.9319	4.7339	High chlorophyll level, healthy and vigorous vegetation.	High chlorophyll level, healthy and vigorous vegetation.
Center	NDVI	0.48275	0.80853	Moderate vegetation.	Temperate and tropical forests.
Center	NDMI	0.06074	0.33809	Medium forest cover, high water stress or medium-low cover, low water stress.	Medium canopy cover, high water stress or medium canopy cover, low water stress.
Center	NDWI	-0.44898	0.020408	Drought, non-aquatic surfaces.	Flooding, humidity.
Center	MSAVI	0.63085	0.89412	Vegetation dense enough to cover the ground.	Vegetation dense enough to cover the ground.
Center	NDRE	0.2967	0.57299	Unhealthy plant or crop not yet mature.	Unhealthy plant or crop not yet mature.
Farm	IC	2.0223	3.9424	High chlorophyll level, healthy and vigorous vegetation.	High chlorophyll level, healthy and vigorous vegetation.
Farm	NDVI	0.47471	0.75636	Moderate vegetation.	Temperate and tropical forests.
Farm	NDMI	0.13339	0.30972	Medium forest cover, high water stress or medium-low cover, low water stress.	Medium canopy cover, high water stress or medium canopy cover, low water stress.
Farm	NDWI	-0.42536	-0.16877	Drought, non-aquatic surfaces.	Moderate drought, non-aquatic surfaces.

Farm	MSAVI	0.65583	0.85838	Vegetation dense enough to cover the ground.	Vegetation dense enough to cover the ground.
Farm	NDRE	0.32	0.54819	Unhealthy plant or crop not yet mature.	Unhealthy plant or crop not yet mature.
North	IC	1.3473	2.5678	High chlorophyll level, healthy and vigorous vegetation.	High chlorophyll level, healthy and vigorous vegetation.
North	NDVI	0.44166	0.73946	Moderate vegetation.	Temperate and tropical forests.
North	NDMI	0.13584	0.32708	Medium forest cover, high water stress or medium-low cover, low water stress.	Medium canopy cover, high water stress or medium canopy cover, low water stress.
North	NDWI	-0.39334	-0.19515	Drought, non-aquatic surfaces.	Moderate drought, non-aquatic surfaces.
North	MSAVI	0.58331	0.80468	Leaf development stage.	Vegetation dense enough to cover the ground.
North	NDRE	0.32012	0.50956	Unhealthy plant or crop not yet mature.	Unhealthy plant or crop not yet mature.
South	IC	0.68947	2.2715	Adequate chlorophyll level, normal growth.	High chlorophyll level, healthy and vigorous vegetation.
South	NDVI	0.32778	0.67321	Moderate vegetation.	Temperate and tropical forests.
South	NDMI	0.081961	0.37262	Medium forest cover, high water stress or medium-low cover, low water stress.	Medium canopy cover, high water stress or medium canopy cover, low water stress.
South	NDWI	-0.23158	0.19302	Moderate drought, non-aquatic surfaces.	Flooding, humidity.
South	MSAVI	0.3289	0.75888	Seed germination stage.	Vegetation dense enough to cover the ground.
South	NDRE	0.13818	0.47754	Bare soil or developing crop.	Unhealthy plant or crop not yet mature.
TAI	IC	1.6007	5.893	High chlorophyll level, healthy and vigorous vegetation.	High chlorophyll level, healthy and vigorous vegetation.
TAI	NDVI	0.37264	0.94906	Moderate vegetation.	Temperate and tropical forests.
TAI	NDMI	0.13898	0.25483	Medium forest cover, high water stress or medium-low cover, low water stress.	Medium canopy cover, high water stress or medium canopy cover, low water stress.
TAI	NDWI	-0.35662	0.14286	Drought, non-aquatic surfaces.	Flooding, humidity.
TAI	MSAVI	0.76082	2.4573	Vegetation dense enough to cover the ground.	Vegetation dense enough to cover the ground.
TAI	NDRE	0.31741	0.96777	Unhealthy plant or crop not yet mature.	Healthy, mature, and ripe crops.

Site 4 (South) shows a moderate density of co-occurrence with species 3 and 4, and a lesser but visible presence of other species such as species 6. Species 1 (Honeybee) and 2 (Wild Bee) appear across all sites with moderate densities but are less dominant compared to Anopheles in sites 1, 2, and 3. Panel (b) displays the density of co-occurrence between species and seasons. It highlights a very strong co-occurrence between species 3 and 4 and season 2 (Minor rainy season), confirming this period as the most favorable for Anopheles proliferation. Season 1 (Minor dry season) shows moderate co-occurrence with species 2, 3, and 4, indicating their presence, though at lower levels. Season 3 (Major dry season) shows low co-occurrence density with Anopheles species but relatively higher density with species 5 (Grasshopper), 6 (Dragonfly), and 7 (Butterfly).

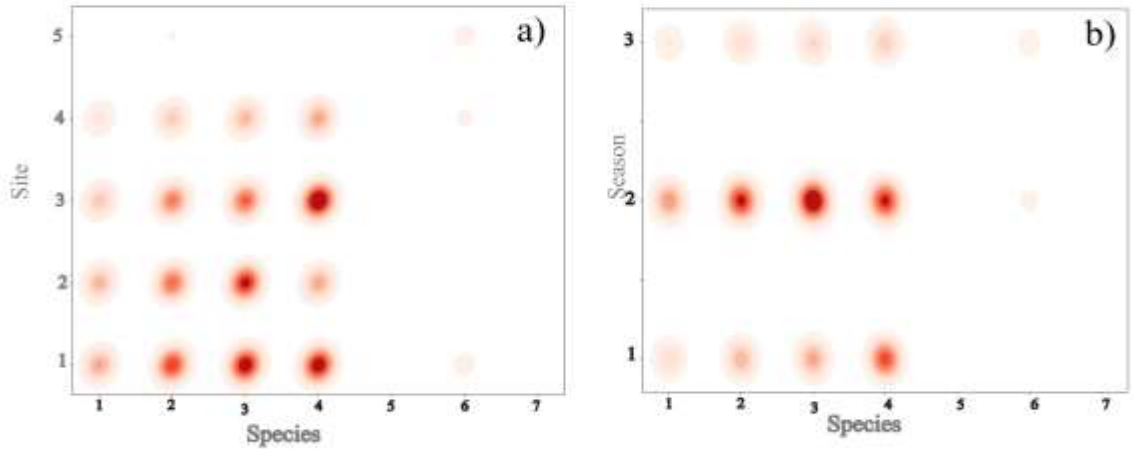

Figure 9. Density of Co-occurrence Between Numeric Values of Species and Site/Season. The figure presents two juxtaposed density heatmaps, visualizing the co-occurrence between the numeric values of species and those of either the sites (a) or the seasons (b). The intensity of the red coloration indicates the most frequently observed combinations. (a) The first heatmap displays the co-occurrence between species (1 to 7) and sites (1 to 5). (b) The second heatmap illustrates the co-occurrence between species and seasons (1 to 3).

In the **Figure 10**, the species 1 (Domestic Bee – 6.3%), 2 (Wild Bee – 9.3%), 3 (Female Anopheles – 33.3%), and 4 (Male Anopheles – 51.1%) are the four most frequently observed species, collectively accounting for a substantial proportion of all captures (**Figure 10-a**). Species 5 (Grasshopper), 6 (Dragonfly), and 7 (Butterfly) are also present in the dataset, but their observation frequency is significantly lower—so much so that their segments are overlapping and not individually distinguishable in this pie chart. Season 2 (Short rainy season) shows an extremely high observation frequency for female Anopheles (8417.63), indicated by a deep red color (**Figure 10-b**). Season 1 (Short dry season) has a significantly lower observation frequency (3015.04), represented by a lighter hue. Season 3 (Long dry season) records the lowest observation frequency for female Anopheles (1308.9), shown in green.

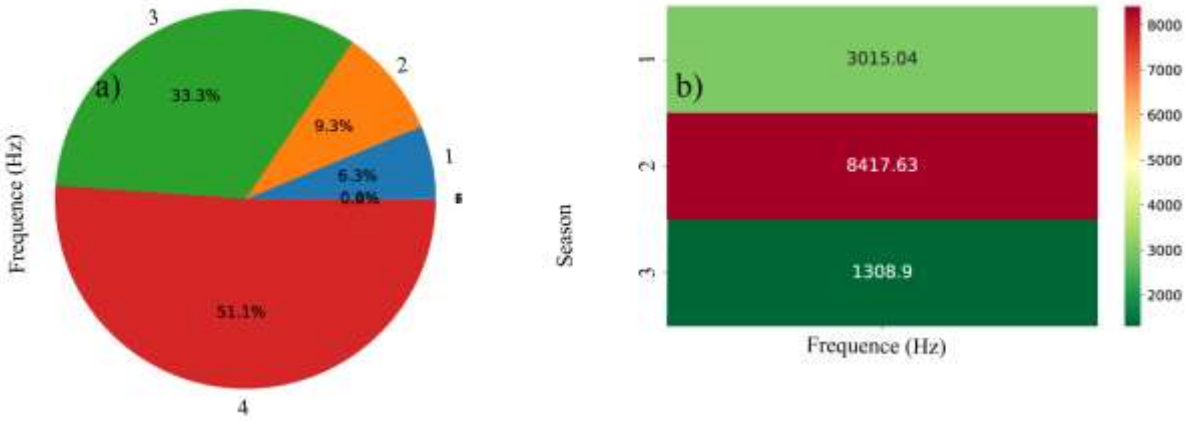

Figure 10. Global distribution of insect species and female Anopheles attraction by season. The pie chart (a) displays the distribution of insect species collected across all sites and seasons. Each slice represents one species (numbered 1 to 7), and its size is proportional to the observation frequency. The percentage for each species is also indicated. On the (b), the heatmap illustrates the seasonal attraction of female Anopheles (species 3). The color intensity (from green to red) reflects the frequency of observations, with numerical values shown for each season (short dry season, short rainy season, long dry season).

4. Discussion

The integrated analysis of Lidar, meteorological, and vegetation index data provides a comprehensive understanding of the spatio-temporal dynamics of *Anopheles* and other insect populations across diverse Ivorian environments. The significance of these findings becomes clearer when compared with established knowledge in the scientific literature.

The observation that *Anopheles* (species 3 and 4) are present across a wide range of temperature and humidity conditions—but appear to favor relatively higher humidity (**Figure 3**)—aligns with existing entomological research. Numerous studies confirm that temperature and humidity are critical factors governing the survival, development, and activity of *Anopheles* mosquitoes (Athni et al. 2024; Beck-Johnson et al. 2013; Christiansen-Jucht et al. 2015; Diouf et al. 2020; Ezihe et al. 2017; Garske et al. 2013). For example, (Ghosh et al. 2024) state that relative humidity above 60% is typically required to prolong adult mosquito survival. Likewise, (Beck-Johnson et al. 2013; Mordecai et al. 2020) modeled the strong thermal dependence of mosquito development and survival rates. Our findings (**Figures 3 and 7**) suggest that local microclimatic conditions strongly influence species distribution—a conclusion also drawn by (Afrane et al. 2012) regarding the effect of microclimates on *Anopheles* fitness.

The pronounced variation in *Anopheles* abundance between sites (**Figure 4-a**)—with higher levels in Center, Farm, and North, and lower levels in the forest site Tai—reflects the influence of land use and habitat heterogeneity on vector populations. Research in Côte d'Ivoire by (N'dri 2023) shows how urbanization and agriculture, particularly rice farming, can create favorable conditions for *Anopheles gambiae s.l.* proliferation (Matthys et al. 2006; Roméo et al. 2022). The lower abundance observed at the forested Tai site (**Figure 4-a**) could reflect less suitable conditions for dominant species like *An. gambiae s.l.*, which prefer sunlit breeding sites (Getachew et al. 2020; Kudom 2015; Yokoly et al. 2021), or it may indicate the presence of more sylvatic species such as *An. nili* (Koffi et al. 2023), though molecular identification would be required to confirm this. Urban-rural-forest comparisons in West Africa often show similar patterns (Fahmy et al. 2015; Taconet et al. 2024).

The marked seasonality in abundance, with a sharp increase during the minor rainy season (Season 2, **Figures 4-b and 5**), is a robust result widely supported by the West African literature (Koffi et al. 2023; Matthys et al. 2006; Soma et al. 2020) and also confirmed in Central Africa (Mayi et al. 2024). For example, (Jawara et al. 2008) documented clear seasonal dynamics, with abundance peaks closely linked to rainfall. The persistent presence of *Anopheles* at the North site even in the late dry season (**Figure 5-b**) is notable and may reflect the presence of more permanent or human-made breeding sites in this peri-urban area, such as rice paddies—consistent with observations by (Kweka et al. 2012; Touré et al. 2019; Zogo et al. 2019) in Korhogo.

The analysis of wingbeat frequency (WBF) using Lidar (**Figure 6**) reveals relatively stable modal and median frequency distributions for *Anopheles* across sites (except Tai) and seasons, despite large fluctuations in abundance. This suggests that the Lidar system consistently detects a group of insects with similar flight characteristics—likely dominant *Anopheles*. This finding supports the utility of WBF for Lidar-based classification, as explored by (Gebru et al. 2015; Jansson et al. 2020), and applied in Côte d'Ivoire by (Kouakou et al. 2020). The stability of WBF distributions, despite environmental changes, implies that these factors primarily affect the size of the active population rather than the dominant species detected.

The observed dusk activity peaks (18:00–20:00) for female *Anopheles* across most sites (**Figure 7**) are well-supported by the literature on African vector behavior. These peaks coincide with times when humans are often outdoors or preparing for bed—key moments for malaria transmission. Lidar studies such as (Jansson et al. 2021) in Tanzania have also captured these crepuscular dynamics at high temporal resolution, confirming the increased activity during twilight. The coincidence of these peaks with still-elevated temperatures and stable or rising humidity (**Figure 7**) reinforces the link between mosquito behavior and immediate microclimatic conditions.

The analysis of abundance in relation to vegetation indices **(Figure 8**) indicates that, although direct 30-minute correlations are not evident, the average habitat characteristics per site are important. Dense vegetation (as shown by high IC, MSAVI, and NDVI values) in sites with high mosquito abundance (Center, Farm, North) supports the known role of vegetation as a resting site for adult mosquitoes and as a potential indicator of favorable microclimates. The importance of agricultural areas (Farm site) is supported by many studies linking rice cultivation or irrigation to high *Anopheles* productivity. The use of indices such as NDVI and NDWI to characterize vector habitats is well-established in remote sensing and malaria risk modeling literature (Liu and Chen 2006; Youssefi et al. 2022).

Lastly, the overall numerical dominance of *Anopheles* (both males and females) in Lidar detections (**Figure 10**) is expected in these malaria-endemic areas, where they are the primary vectors. The high proportion of male detections may be due to the Lidar method itself (which is less biased toward biting females) or the proximity of Lidar transects to swarming sites—a behavior primarily exhibited by males and detectable by Lidar, as observed by (Jansson et al. 2021).

A key advantage of this study lies in its capacity to enable early surveillance using this method. However, a major limitation is the processing of imagery for calculating vegetation indices. Without proficiency in programming languages such as JavaScript and Python, it becomes challenging to filter the data effectively—especially to remove cloud interference and retain only relevant ground-level information.

5. Conclusions

In conclusion, this study demonstrates the feasibility and utility of an integrated approach combining Scheimpflug Lidar data, meteorological data, and vegetation indices for high-resolution monitoring of Anopheles populations in Côte d'Ivoire. The results show that vector activity varies by location and time, with clear peaks depending on the seasons and between day and night. They also indicate that local weather and habitat characteristics, such as vegetation, have a significant influence on their numbers and activity. Variations in weather conditions (temperature, humidity) and vegetation indices, measured by remote sensing (Lidar, multispectral images), are closely linked to the abundance and activity of Anopheles mosquitoes in the different environments studied in Côte d'Ivoire. Future research should consider the use of multispectral drones for soil mapping in order to overcome the interference barrier related to cloud cover, thereby retaining more accurate and relevant information.

Acknowledgments

We would like to express our sincere gratitude and deep appreciation to the African Spectral Imaging Network (AFSIN) for funding this study, as well as to Carla Puglia, coordinator of the

International Science Programme in Uppsala, for her continuous support. Our thanks also go to the Swedish team for their assistance and invaluable support. We are deeply grateful to the Félix Houphouët-Boigny National Polytechnic Institute (INP-HB) for generously allowing most of the measurements to be conducted across the institute's various sites, and to the forest rangers of the Taï Forest for their help and support in the Taï primary rainforest.

Disclosure statement*: Conflict of Interest:* The authors declare that there are no conflicts of interest. *Compliance with Ethical Standards:* This article does not contain any studies involving human or animal subjects.

References

Achee, N. L., Grieco, J. P., Masuoka, P., Andre, R. G., Roberts, D. R., Thomas, J., et al. (2006). Use of remote sensing and geographic information systems to predict locations of Anopheles darlingi-positive breeding sites within the Sibun River in Belize, Central America. *Journal of medical entomology*, *43*(2), 382–392.

Adja, A. M., Assouho, K. F., Assi, S.-B., Guindo-Coulibaly, N., Tia, E., Sagna, A. B., et al. (2022). High vectorial transmission of malaria in urban and rural settings in the northern, western and eastern regions of Côte d'Ivoire. *Journal of Vector Borne Diseases*, *59*(3), 275–284.

Afrane, Y. A., Githeko, A. K., & Yan, G. (2012). The ecology of *Anopheles* mosquitoes under climate change: case studies from the effects of deforestation in East African highlands. *Annals of the New York Academy of Sciences*, *1249*(1), 204–210. https://doi.org/10.1111/j.1749-6632.2011.06432.x

Amin I.S., Amin H.S. (2024). Enhancing the Applicability and Development of Vegetation Indices for Mangroves, *JSDSES*, 3(2), 58-72, https://doi.org/10.21608/jsdses.2024.305202.1034

Athni, T. S., Childs, M. L., Glidden, C. K., & Mordecai, E. A. (2024). Temperature dependence of mosquitoes: Comparing mechanistic and machine learning approaches. *PLOS Neglected Tropical Diseases*, *18*(9), e0012488.

Beck-Johnson, L. M., Nelson, W. A., Paaijmans, K. P., Read, A. F., Thomas, M. B., & Bjørnstad, O. N. (2013). The effect of temperature on Anopheles mosquito population dynamics and the potential for malaria transmission. *PLOS one*, *8*(11), e79276.

Brydegaard, M., Jansson, S., Malmqvist, E., Mlacha, Y. P., Gebru, A., Okumu, F., et al. (2020). Lidar reveals activity anomaly of malaria vectors during pan-African eclipse. *Science Advances*, *6*(20), eaay5487–eaay5487.

Chaki, P. P., Mlacha, Y., Msellemu, D., Muhili, A., Malishee, A. D., Mtema, Z. J., et al. (2012). An affordable, quality-assured community-based system for high-resolution entomological surveillance of vector mosquitoes that reflects human malaria infection risk patterns. *Malaria Journal*, *11*(1), 172. https://doi.org/10.1186/1475-2875-11-172

Christiansen-Jucht, C., Erguler, K., Shek, C. Y., Basáñez, M.-G., & Parham, P. E. (2015). Modelling Anopheles gambiae ss population dynamics with temperature-and age-dependent survival. *International journal of environmental research and public health*, *12*(6), 5975–6005.

Diouf, I., Fonseca, B. R., Caminade, C., Thiaw, W. M., Deme, A., Morse, A. P., et al. (2020). Climate variability and malaria over West Africa. *The American Journal of Tropical Medicine and Hygiene*, *102*(5), 1037.

Djamouko-Djonkam, L., Mounchili-Ndam, S., Kala-Chouakeu, N., Nana-Ndjangwo, S. M., Kopya, E., Sonhafouo-Chiana, N., et al. (2019). Spatial distribution of Anopheles gambiae sensu lato larvae in the urban environment of Yaoundé, Cameroon. *Infectious Diseases of Poverty*, *8*(1), 84. https://doi.org/10.1186/s40249-019-0597-6

Ezihe, E. K., Chikezie, F. M., Egbuche, C. M., Nwankwo, E. N., Onyido, A. E., Aribodor, D., & Samdi, M. L. (2017). Seasonal distribution and micro-climatic factors influencing the abundance of the malaria vectors in south-east Nigeria. *Journal of mosquito research*, *7*(3). https://www.researchgate.net/profile/Chukwuebuka-Ezihe/publication/315349309_Seasonal_Distribution_and_Micro-Climatic_Factors_Influencing_the_Abundance_of_the_Malaria_Vectors_in_South-East_Nigeria/links/5a96826aa6fdccecff095765/Seasonal-Distribution-and-Micro-Climatic-Factors-Influencing-the-Abundance-of-the-Malaria-Vectors-in-South-East-Nigeria.pdf?_sg%5B0%5D=started_experiment_milestone&origin=journalDetail. Accessed 14 April 2025

Fahmy, N. T., Villinski, J. T., Bolay, F., Stoops, C. A., Tageldin, R. A., Fakoli, L., et al. (2015). The seasonality and ecology of the Anopheles gambiae complex (Dipetra: Culicidae) in Liberia using molecular identification. *Journal of medical entomology*, *52*(3), 475–482.

Fournet, F., Adja, A. M., Adou, K. A., Dahoui, M. M., Coulibaly, B., Assouho, K. F., et al. (2022). First detection ofthemalaria vector Anopheles arabiensis inCôte d'Ivoire: urbanization inquestion. https://media.malariaworld.org/s12936_022_04295_3_354717f348.pdf. Accessed 12 April 2025

Frake, A. N., Peter, B. G., Walker, E. D., & Messina, J. P. (2020). Leveraging big data for public health: Mapping malaria vector suitability in Malawi with Google Earth Engine. *PLoS One*, *15*(8), e0235697.

Garske, T., Ferguson, N. M., & Ghani, A. C. (2013). Estimating air temperature and its influence on malaria transmission across Africa. *PloS one*, *8*(2), e56487.

Gbogbo, A. Y., Kouakou, B. K., Dabo-Niang, S., & Zoueu, J. T. (2022). Predictive model for airborne insect abundance intercepted by a continuous wave Scheimpflug lidar in relation to meteorological parameters. *Ecological Informatics*, *68*, 101528. https://doi.org/10.1016/j.ecoinf.2021.101528

Gebru, A., Brydegaard, M., Rohwer, E., & Neethling, P. (2015). Applied kHz optical remote sensing for determination of insect flight direction and relative size. In *Laser Science* (pp. JTu4A-54). Optica Publishing Group.

Getachew, D., Balkew, M., & Tekie, H. (2020). Anopheles larval species composition and characterization of breeding habitats in two localities in the Ghibe River Basin, southwestern Ethiopia. *Malaria Journal*, *19*(1), 65. https://doi.org/10.1186/s12936-020-3145-8

Ghosh, C., Kumar, N., Mogaveerthi, S., Lamba, S., Ramanjini, C. K., Joshi, S. G., et al. (2024). Effects of temperature and nutrition stress on Anopheles stephensi, an Indian urban malaria vector. https://www.researchsquare.com/article/rs-5214107/latest. Accessed 14 April 2025

Jansson, S., Malmqvist, E., Brydegaard, M., Åkesson, S., & Rydell, J. (2020). A Scheimpflug lidar used to observe insect swarming at a wind turbine. *Ecological Indicators*, *117*, 106578–106578.

Jansson, S., Malmqvist, E., Mlacha, Y., Ignell, R., Okumu, F., Killeen, G., et al. (2021). Real-time dispersal of malaria vectors in rural Africa monitored with lidar. *PLOS ONE*, *16*(3), e0247803. https://doi.org/10.1371/journal.pone.0247803

Jawara, M., Pinder, M., Drakeley, C. J., Nwakanma, D. C., Jallow, E., Bogh, C., et al. (2008). Dry season ecology of Anopheles gambiae complex mosquitoes in The Gambia. *Malaria Journal*, *7*(1), 156. https://doi.org/10.1186/1475-2875-7-156

Koffi, A. A., Camara, S., Ahoua Alou, L. P., Oumbouke, W. A., Wolie, R. Z., Tia, I. Z., et al. (2023). Anopheles vector distribution and malaria transmission dynamics in Gbêkê region, central Côte d'Ivoire. *Malaria Journal*, *22*(1), 192. https://doi.org/10.1186/s12936-023-04623-1

Kouakou, B. K., Jansson, S., Brydegaard, M., & Zoueu, J. T. (2020). Entomological Scheimpflug lidar for estimating unique insect classes in-situ field test from Ivory Coast. *OSA Continuum*, *3*(9), 2362–2371. https://doi.org/10.1364/OSAC.387727

Kudom, A. A. (2015). Larval ecology of Anopheles coluzzii in Cape Coast, Ghana: water quality, nature of habitat and implication for larval control. *Malaria Journal*, *14*(1), 447. https://doi.org/10.1186/s12936-015-0989-4

Kweka, E. J., Zhou, G., Munga, S., Lee, M.-C., Atieli, H. E., Nyindo, M., et al. (2012). Anopheline larval habitats seasonality and species distribution: a prerequisite for effective targeted larval habitats control programmes. *PloS one*, *7*(12), e52084.

Laita M., Hammouti B., Sabbahi R., Messaoudi Z., Benkirane R. (2024) Effect of Water Regime and Soil Maintenance Mode on Vegetative Growth and Peach Tree Production, *Indonesian Journal of Science & Technology*, 9(1), 33-44

Le Breton, C., Laporta, G. Z., Sallum, M. A. M., Hesse, H., Salgado-Lynn, M., Manin, B. O., & Fornace, K. (2025). Advancing canopy-level entomological surveillance to monitor vector-borne and zoonotic disease dynamics. *Trends in Parasitology*. https://www.cell.com/trends/parasitology/abstract/S1471-4922(24)00371-4. Accessed 13 April 2025

Li, M. (2024). Coherent Backscattering from Free-Flying Insects: Implications for Remote Species Identification. https://portal.research.lu.se/files/194434756/Thesis_Meng_Li_LUCRIS.pdf. Accessed 27 March 2025

Liu, J., & Chen, X. (2006). Relationship of Remote Sensing Normalized Differential Vegetation Index to Anopheles Density and Mlaria Incidence Rate. *Biomedical and Environmental Sciences*, *19*(2), 130.

Manta, R. M. (2025). malaria in Ivory Coast. https://www.severemalaria.org/en/node/1575. Accessed 12 April 2025

Matthys, B., N'Goran, E. K., Koné, M., Koudou, B. G., Vounatsou, P., Cissé, G., et al. (2006). Urban agricultural land use and characterization of mosquito larval habitats in a medium-sized town of Cote d'Ivoire. *Journal of Vector Ecology*, *31*(2), 319–333.

Mayi, M. P. A., Kowo, C., Forfuet, F. D., Anong, D. N., Fonda, A. E., Elad, M., et al. (2024). Water sources selected for immature development of some African rainforest dwelling mosquitoes under different landscapes in Cameroon. *Journal of Medical Entomology*, tjae146.

Mordecai, E. A., Ryan, S. J., Caldwell, J. M., Shah, M. M., & LaBeaud, A. D. (2020). Climate change could shift disease burden from malaria to arboviruses in Africa. *The Lancet Planetary Health*, *4*(9), e416–e423.

N'dri, B. P. (2023). *Malaria transmission and insecticide resistance in Anopheles gambiae in Ellibou, Côte d'Ivoire* (PhD Thesis). University_of_Basel. Retrieved from https://edoc.unibas.ch/94965/

Roméo, N. N., Lucien, K. Y., Ibrahima, C. Z., Urbain, S. G., Ladji, Y. K., & Eliezer, N. K. (2022). Identification and characterization of Anopheles Breeding habitats in Dabakala, Central-East Cote d'Ivoire. *Journal of Entomology and Zoology Studies*, *10*(2), 181–189. https://doi.org/10.22271/j.ento.2022.v10.i2c.8985

Soma, D. D., Zogo, B. M., Somé, A., Tchiekoi, B. N., Hien, D. F. de S., Pooda, H. S., et al. (2020). Anopheles bionomics, insecticide resistance and malaria transmission in southwest Burkina Faso: a pre-intervention study. *PloS one*, *15*(8), e0236920.

Stein, M., Martin, M. E., Ramírez, P. G., Etchepare, E. G., Oria, G. I., Rossi, G. C., et al. (2023). Updated Anopheles mosquitos abundance and distribution in north-eastern malaria-free area of Argentina. *Anais da Academia Brasileira de Ciências*, *95*(suppl 2), e20220956.

Taconet, P., Zogo, B., Ahoua Alou, L. P., Amanan Koffi, A., Dabiré, R. K., Pennetier, C., & Moiroux, N. (2024). Landscape and meteorological determinants of malaria vectors' presence and abundance in the rural health district of Korhogo, Côte d'Ivoire, 2016–2018, and comparison with the less anthropized area of Diébougou, Burkina Faso. *PloS one*, *19*(10), e0312132.

Tahir, F., Bansal, D., Rehman, A. ur, Ajjur, S. B., Skariah, S., Belhaouari, S. B., et al. (2023). Assessing the impact of climate conditions on the distribution of mosquito species in Qatar. *Frontiers in Public Health*, *10*, 970694.

Touré, D. S., Ouattara, A. F., Doumbia, M., Danon, A. S. D., Kwadjo, K. E., Kra, K. D., et al. (2019). Typology of domestic larval habitats of Anopheles in the rural savanna of northern Côte d'Ivoire. https://www.researchgate.net/profile/Mamadou-Doumbia/publication/333485755_Typology_of_domestic_larval_habitats_of_Anopheles_in_the_rural_savanna_of_northern_Cote_d'Ivoire/links/5cefdd9e299bf1fb184a9823/Typology-of-domestic-larval-habitats-of-Anopheles-in-the-rural-savanna-of-northern-Cote-dIvoire.pdf. Accessed 14 April 2025

USAID. (2024). Côte d'Ivoire | PMI Evolve. https://pmievolve.org/cote-divoire. Accessed 12 April 2025

Yokoly, F. N., Zahouli, J. B. Z., Small, G., Ouattara, A. F., Opoku, M., De Souza, D. K., & Koudou, B. G. (2021). Assessing Anopheles vector species diversity and transmission of malaria in four health districts along the borders of Côte d'Ivoire. *Malaria Journal*, *20*(1), 409. https://doi.org/10.1186/s12936-021-03938-1

Youssefi, F., Javad Valadan Zoej, M., Ali Hanafi-Bojd, A., Borahani Dariane, A., Khaki, M., & Safdarinezhad, A. (2022). Predicting the location of larval habitats of Anopheles mosquitoes using remote sensing and soil type data. *International Journal of Applied Earth Observation and Geoinformation*, *108*, 102746. https://doi.org/10.1016/j.jag.2022.102746

Zogo, B., Koffi, A. A., Alou, L. P. A., Fournet, F., Dahounto, A., Dabiré, R. K., et al. (2019). Identification and characterization of Anopheles spp. breeding habitats in the Korhogo area in northern Côte d'Ivoire: a study prior to a Bti-based larviciding intervention. *Parasites & Vectors*, *12*(1), 146. https://doi.org/10.1186/s13071-019-3404-0